Possibilities for monitoring the composition of an iPWR core using ex-core neutron detectors

Markus Preston[1], Erik Branger[1], Sophie Grape[1], Olena Khotiaintseva[1,2], Volodymyr Khotiaintsev[1,3]

[1] Department of Physics and Astronomy, Uppsala University, Uppsala, Sweden

[2] Institute for Safety Problems of Nuclear Power Plants of the NAS of Ukraine, Kyiv, Ukraine

[3] Taras Shevchenko National University of Kyiv, Kyiv, Ukraine

Abstract

The possibility for wide-spread implementation of small modular reactors (SMRs) in the coming years comes with associated challenges for international nuclear safeguards: more effective and efficient use of safeguards resources will be needed and safeguards methodologies for monitoring SMRs may need to be developed. Of particular interest are methods for unattended monitoring, which could complement on-site inspections at facilities. One possibility for remote monitoring is using neutron detectors to determine the time-evolution of the core fissile composition. Although ex-core neutron detectors are commonly used in nuclear power plants to monitor the short-term behaviour of the core, this technique would be based on long-term monitoring over one or more operating cycles.

In this work, we investigate the possibilities for using ex-core neutron detectors to monitor the long-term composition of a 160 MW_{th} NuScale integral pressurised water reactor (iPWR) core. This core was chosen as a first case study, given the wide spectrum of SMR concepts. The considered iPWR module is housed in a pool of borated water, which significantly affects the neutron flux outside the reactor. Depletion calculations in Serpent2 have been performed for a 2D model of the core to determine the evolution of the fuel composition over a two-year operating cycle. Using variance reduction techniques, the thermal and fast neutron fluxes were determined at various distances into the water outside the iPWR module. Changes in the ex-core neutron flux and its relationship to the flux in the core with fuel depletion were studied. It was found that the relationship between the ex-core neutron flux and the flux in the core changes during depletion. Different possible sources to these changes were studied to investigate the validity of the proposed safeguards monitoring technique for an iPWR module housed in water.

Keywords: Nuclear safeguards, small modular reactor, neutron monitoring, fissile composition

1. Introduction

There is currently a significant interest in a number of different small modular reactor (SMR) concepts, which potentially could offer benefits in terms of type licensing and shorter construction times, as well as flexibility in power generation and geographic placement. This flexibility could lead to reactors being deployed in new and possibly remote locations. Factors such as this, along with possibly relatively long operating cycles, have been identified as a potential challenge to nuclear safeguards [1]. Recent years have seen a growing interest in

developing radiation-detection techniques for monitoring parameters such as power level and core composition during operation of a reactor [2-3]. Applying such techniques for monitoring SMRs could be one way of reducing the time and cost associated with inspections while fulfilling safeguards objectives. The development of techniques that perform unattended monitoring over time also align well with aims for future IAEA safeguards [4].

Of particular interest for this work, [3] proposes monitoring the average fissile composition of a reactor core by detecting neutrons leaking from the core. One of the assumptions made in that work is that the detection rate in an ex-core neutron detector, n_{det}, is proportional to the average neutron flux inside the core, $\langle\phi\rangle_{core}$:

$$n_{det} \propto \langle\phi\rangle_{core} \tag{1}$$

In this work, we investigate whether Eq. 1 is valid over a two year long irradiation cycle in an SMR. Monte Carlo simulations have been used to estimate how the neutron flux outside a 160-MW_{th} NuScale integral pressurised water reactor (iPWR) [5] changes with time when the reactor is operated at a constant power level.

2. Theory

We assume that the detection rate n_{det} is directly related to the flux ϕ_{det} at the ex-core detector location and adopt a very general expression for ϕ_{det}, adapted from [6] to yield the ex-core flux:

$$\phi_{det}(E, \bar{r}) = \int_V d\bar{r}_0 \int_0^\infty dE_0 w(E_0 \rightarrow E, \bar{r}_0 \rightarrow \bar{r}) S(E_0, \bar{r}_0), \tag{2}$$

where E_0 is the energy of a neutron emitted at a point $\bar{r}_0$ in the core and S is the neutron emission rate per energy and volume at that point. Each point in the core has an associated weighting function w — the probability that a neutron emitted at this point with this energy will contribute to the flux with an energy E at the detector located at $\bar{r}$. In practical terms, this equation means that the neutron flux outside the core is not only related to the amplitude of S in the core, but also to some extent to its spatial and energy distribution. The values of w will depend on the ex-core detector and its placement in relation to the core.

The thermal power generated in the core may be written as:

$$P_{core} = \int_V d\bar{r}_0 \langle\phi\rangle(\bar{r}_0) \sum_i N_i(\bar{r}_0) \langle\sigma_{f,i}\rangle E_{f,i}, \tag{3}$$

where ϕ is the space-dependent neutron flux in the core. Here, we have averaged over the incident-neutron energy spectrum at each position $\bar{r}_0$ at time t. The sum over i is for the fissioning nuclides in the core, which each has a number density N, a fission cross section $\sigma_{f,i}$ and an associated average energy release per fission $E_{f,i}$. Several of these parameters may vary with time. When fuel is depleted during irradiation, the fissile composition will change. In order

to maintain a constant reactor power, also the neutron flux in the core will slowly change with time. This is the main point behind the neutron-monitoring approach proposed in [3]: if the core power output (assumed to be proportional to P_{core}) is known, the time-dependence of the detected neutron flux ϕ_{det} can provide information about the fissile composition of the core. We emphasise that the time-dependencies discussed here are on relatively long time-scales due to fuel depletion.

Going back to Eq. 2, the neutron emission rate S per unit energy and volume at a certain point in the core may be written in terms of the (one-group) neutron flux at that point:

$$S(E_0, \overline{r_0}) = \langle\phi\rangle(\overline{r_0}) \sum_i N_i(\overline{r_0})\langle\sigma_{f,i}\rangle\bar{\nu}_i\langle\chi_i\rangle(E_0), \quad (4)$$

where $\bar{\nu}$ is the average number of neutrons released per fission and χ is the energy spectrum of fission neutrons. Again, we have averaged over the incident-neutron energy spectrum at $\overline{r_0}$. When the power level is changed at a given point in time, the amplitude of the $\langle\phi\rangle$ and S distributions will scale linearly. However, when fuel is depleted, the terms inside the sum in Eq. 4 will change but so will $\langle\phi\rangle$. It is clear that the spatial distribution of S will be coupled to the spatial power and flux distributions. This is of relevance in this context, since Eq. 2 states that the neutron flux detected outside the core will be sensitive to the spatial distribution of S (assuming that the weighting functions w are constant over time). We expect the weighting functions to be skewed towards the periphery of the core — a neutron emitted near the core periphery will have a higher probability of reaching an ex-core detector than a neutron emitted in the core centre. That is, changes in the power and flux distribution will affect which fraction of the core neutron flux distribution is "seen" by detector(s) placed outside the core. This would in turn mean that the ratio $\phi_{det}/\langle\phi\rangle_{core}$ may not be constant over time. Should this be the case Eq. 1, proposed in [3], may not be time-independent over an entire irradiation cycle.

We emphasise that if the monitoring technique is to be fully independent of operator declarations, many of the parameters in Eq. 4 will not be known *a priori* by the safeguards inspectorate. This marks a contrast with the use of ex-core monitors by a reactor operator, where changes in core composition and flux distribution can be corrected for by re-calibration.

3. Model

3.1. NuScale power module

In this work, we study the neutron leakage from a single NuScale module with a thermal power of 160 MW_{th}. Although there exist a number of SMR concepts, we selected this one due to the relatively large amount of publicly available design information [5]. It should be noted that these data are for the 160 MW_{th} reactor design, and that they and the results of this work do not reflect the 250 MW_{th} NuScale reactor design. The NuScale concept described in [5] involves a number of individual reactor modules located in water below ground level. This water is shared between the reactor pool, the spent-fuel pool and the refuelling pool and will, for reasons of criticality safety, contain boron at a concentration of 1800 ppm. Each reactor module is housed in a 6-m

wide bay surrounded by concrete on three sides [5]. Because we only study the radial dependence of the neutron flux outside the CNV, and in the interest of computational time, an axially infinite geometry was modelled. The modelled geometry is shown in Fig. 1, and includes the core, reflector, pressure vessel (PV), containment vessel (CNV) and pool water to the edge of the module bay. Most parameters relating to geometry and structural materials were adopted from openly available licensing documents for the NuScale design [5]. The fuel was surrounded by a thick reflector made from SS-304 stainless steel, which was also used for the PV. As described in Sec. 4.1, a time-dependent concentration of soluble boron was used in the coolant water inside the core. The same water composition was used in the downcomer between the reflector and the PV. The CNV (made from SA-965 steel) surrounds the PV and has an outer radius of 179 cm. Finally, water with a fixed boron concentration of 1800 ppm surrounds the CNV to the edge of the geometry.

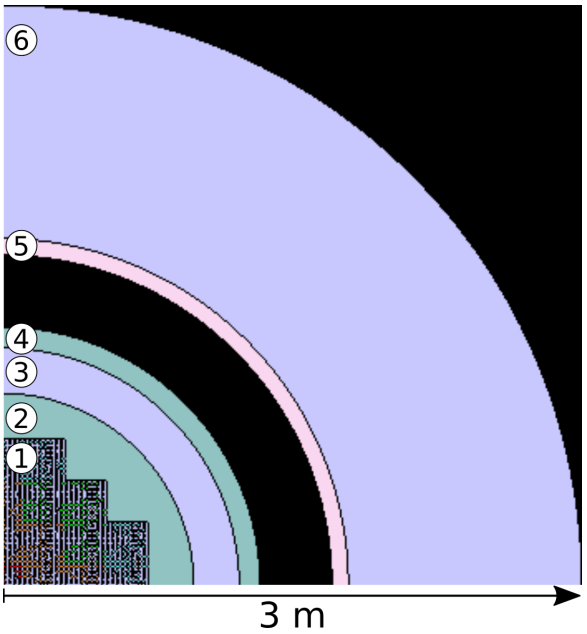

Figure 1: Top view of a quarter of the axially infinite core model implemented in Serpent2. From the centre outwards: (1) the core, (2) steel reflector and barrel, (3) water-filled downcomer, (4) PV, (5) CNV and (6) reactor pool. The outer edge of the modelled cylindrical geometry is 3 metres from the core centre.

3.2. Core

The fuel composition used in this work was obtained from [7]. The modelled core consisted of 37 17x17 fuel assemblies with varying enrichments ranging from 1.95% (in the core centre) to 3.60% (in the core periphery). Each fuel assembly contains 25 water channels. As described in [7], some of the fuel assemblies contained eight gadolinium-bearing fuel pins acting as burnable absorbers. We simulate only the very first 2-year cycle with this core, i.e. all fuel assemblies start as fresh fuel, thus the fuel has not reached an equilibrium core configuration. The fresh core composition is listed in Table 1.

Table 1: Composition of the fresh fuel in the modelled core.

Fuel assembly type	**Composition**	**Assemblies in core**
A	264 pins with 1.95 wt-% U-235	1
B	264 pins with 2.05 wt-% U-235	12
C	264 pins with 2.70 wt-% U-235	4
D	264 pins with 3.60 wt-% U-235	8
E	256 pins with 2.70 wt-% U-235 8 pins with 1.8 wt-% U-235 and 2.5% Gd	8
F	256 pins with 3.60 wt-% U-235 8 pins with 1.5 wt-% U-235 and 3.0% Gd	4

4. Method

4.1. Depletion calculations

The Monte Carlo code Serpent2 [8] was used to perform depletion calculations on an axially infinite model of the NuScale core. The symmetry of the geometry was utilised by only defining 1/8 of the core in Serpent2 and applying symmetry conditions to yield the full core. In the depletion calculation, the modelled geometry extended only to the reactor PV, with the assumption that material outside this has little impact on the core neutronics. The depletion calculation was performed in time steps of 20 days up to 2 years. Each time step involved a criticality calculation with 10^5 neutrons per cycle for 100 inactive and 1000 active cycles. The number of cycles and source neutrons was selected after evaluating criticality-source convergence criteria in Serpent. Each fuel assembly was defined as a depletion zone, meaning that nuclide concentrations were updated on an assembly, rather than pin-wise, level. An exception to this were the gadolinium-bearing pins, which each consisted of 10 radial depletion zones to accurately model the radial burnout of gadolinium. Equilibrium xenon and samarium levels were determined separately by Serpent. The depletion calculations were normalised to a constant linear power generation of 0.8 MW_{th}/cm, assuming that the core has an active height of 200 cm. ENDF-B/VII.1 nuclear data were used. In order to maintain a constant $k_{eff} = 1$ throughout the cycle, the equilibrium boron concentration in the core was calculated by Serpent at each depletion step. This was done to imitate the effect of reactivity control over the cycle.

4.2. Neutron-transport calculations

In this work, we are interested in time-dependent variations in the neutron flux outside the CNV. For this part of the modelling, the geometry was extended beyond the PV, as shown in Fig. 1. Instead of selecting a specific neutron detector, which would have a certain response function, we investigate the neutron flux at different radial distances into the water outside the CNV. This could serve as a basis for future selection of an appropriate neutron detector for the considered monitoring task. In the modelled geometry, multiple layers of metal and borated water will attenuate the neutron flux outside the reactor core by several orders of magnitude. To accurately estimate the radial and spectral distribution of neutrons outside the CNV, a direct Monte Carlo

calculation would require simulating a very large number of neutron histories. Instead, we applied the weight-window based global variance reduction technique in Serpent2 [9] to reduce the variance in flux estimates outside the CNV. This was done by a two-step approach:

- The core fission source term had to be determined. Because this was not saved to file during the depletion calculations, additional criticality calculations were performed with the extended geometry at three points in time: beginning-of-cycle (BOC, 0 days), middle-of-cycle (MOC, 365 days) and end-of-cycle (EOC, 730 days). For each time step, the material compositions were obtained from the depletion calculations described above. For each calculation, the neutron source term was written to a file.
- In a subsequent run, the source term was used as an external source and neutron transport simulated and variance reduction optimised and applied to obtain neutron-flux estimates outside the CNV. For this run, 10^8 initial histories were simulated. Additional neutron generation in fission reactions was disabled since the fission source term from the criticality calculation already includes this. Global variance reduction with a cylindrical weight window mesh was used, with four iterations to optimise the weight windows.

Using the appropriate flux tallies in Serpent2, the spatial and energy distributions of the neutron flux in the water outside the CNV were obtained. Because the modelled reactor is axially infinite, no axial dependence has been studied. Furthermore, the flux tallies covered the full 360° around the core, meaning that no azimuthal dependence has been studied (because the core is not fully cylindrically symmetric, some azimuthal dependence may be expected in reality). Each tally was separated into a thermal (<0.625 eV) and a fast (≥ 0.625 eV) energy group.

5. Analysis and Results

5.1. Neutron flux outside the CNV

Fig. 2 shows the thermal-group and fast-group neutron flux outside the CNV at different distances from the core centre, at three points in time during the irradiation cycle. Due to the high boron concentration in the water outside the CNV, the thermal-neutron absorption outside the CNV is significant. As a result, neutrons which have thermalised before leaking out of the core will only have a short mean free path in the water. We note that at some distance into the water, the thermal and fast flux start to follow approximately the same radial dependence, indicating that thermal neutrons at a detector located this far from the core have scattered from fast to thermal energies relatively close to the detector. Overall, the neutron flux increases by approximately 12% during the two-year cycle. An increased flux over time is expected, given that the average fissile composition decreases over time and the core power is fixed. Although not studied in detail here, we notice a slight variation in this increase with radial distance, which might be due to the fact that different radial distances have different associated weighting functions (see Eq. 2). This means that the detector location to some extent impacts how well different regions of the core are probed. Nonetheless, the 12% increase over the cycle appears to stay constant at distances longer than ~220 cm. These results could be used as a first basis for selecting a detector which can operate in a certain neutron flux while allowing a sufficiently low statistical uncertainty during measurement times on the order of a day per datum point. We note that a detector placed further from the core, as in [3], will require longer measurement times and likely result in a more complex combination of materials between the core and detector.

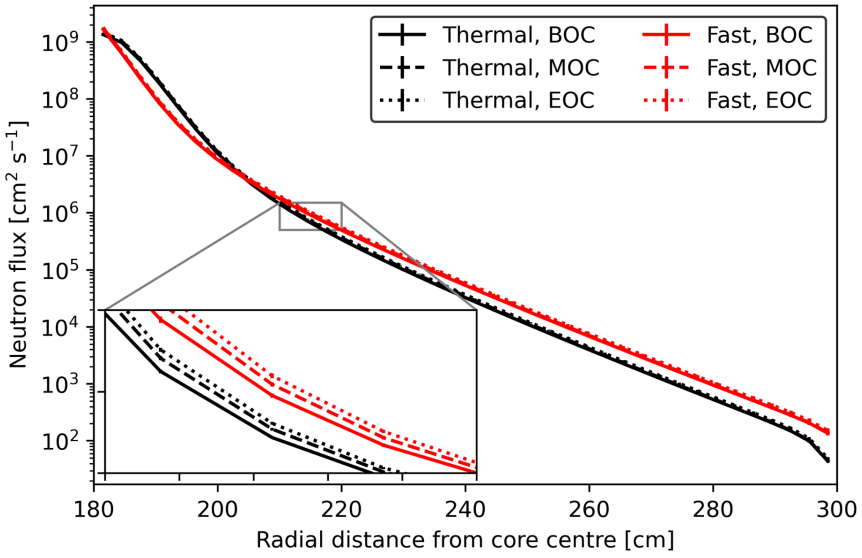

Figure 2: The thermal-group (<0.625 eV) and fast-group (≥0.625 eV) neutron flux as function of the distance from the core centre. The CNV outer edge is located at r=179 cm. Data are shown for three points in time in the irradiation cycle: BOC (0 days), MOC (365 days) and EOC (730 days). The inset shows a ~12% increase in flux during the considered cycle.

5.2. Neutron flux outside the CNV compared to the core-averaged flux

If Eq. 1 is to be applicable here, the ratio $\langle\phi\rangle_{det}/\langle\phi\rangle_{core}$ is expected to be independent of time. To study this ratio, the total neutron flux $\langle\phi\rangle_{det}$ was determined at the three points in time in a 10-cm wide radial bin centred at r_{det}=215 cm (35 cm from the CNV). $\langle\phi\rangle_{core}$ was determined by tallying the total neutron flux in the reactor fuel at each point in time. As shown in Fig. 3, we note an increase in the ratio of approximately 8% over the cycle, indicating that Eq. 1 is not fully valid. A change in $\langle\phi\rangle_{det}$ could therefore indicate either a change in $\langle\phi\rangle_{core}$, a change in the ratio or both. We now proceed to study whether this can be attributed to a time-dependent spatial distribution of the neutron production rate S.

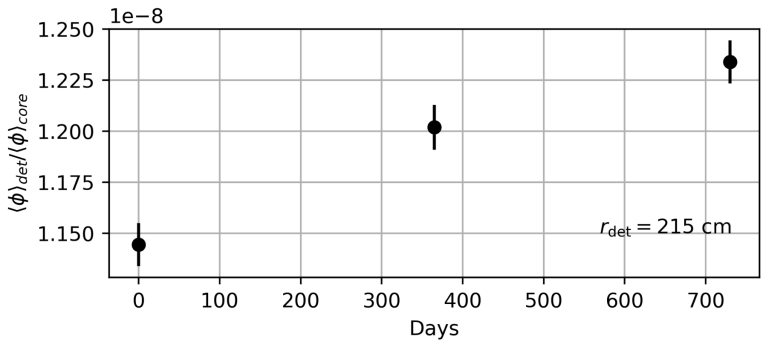

Figure 3: The ratio between the total neutron flux at r_{det}=215 cm and the core-averaged flux at three points in time. Eq. 1 assumes this ratio to be time-independent, however here we note an increase by 8% over the modelled two-year cycle. Error bars show the statistical uncertainties.

5.3. Spatial distribution of the neutron-production rate

Based on Eqs. 2 and 4, a time-dependent ratio $\langle\phi\rangle_{det}/\langle\phi\rangle_{core}$ seen in Fig. 3 can be due to changes in the weighting functions w or in the spatial distribution of S with time. In this work, we assume that the weighting functions (w) are independent of time. In order to study the impact of variations in the spatial distribution of S, the assembly-wise ratio $S/\langle\phi\rangle_{core}$ was determined at three points in the irradiation cycle: 0 days, 365 days and 730 days. S was determined for each fuel assembly by tallying the fission-neutron production rate in the fuel. The results are shown in Fig. 4. These results show that during the modelled irradiation cycle there is a shift in the spatial distribution of S, which is connected to shifts in the power and flux distributions in the core. There are several reasons for this, including fuel and gadolinium depletion and plutonium breeding. That is, the average fissile composition of the core not only impacts the relationship between $\langle\phi\rangle_{core}$ and the core power, but also between S and $\langle\phi\rangle_{core}$. In the peripheral FAs (which have the highest weighting functions w), the relative increase in $S/\langle\phi\rangle_{core}$ is up to 6%, depending on the FA. This could be one of the explanations for the increase in the ratio $\langle\phi\rangle_{det}/\langle\phi\rangle_{core}$ over time.

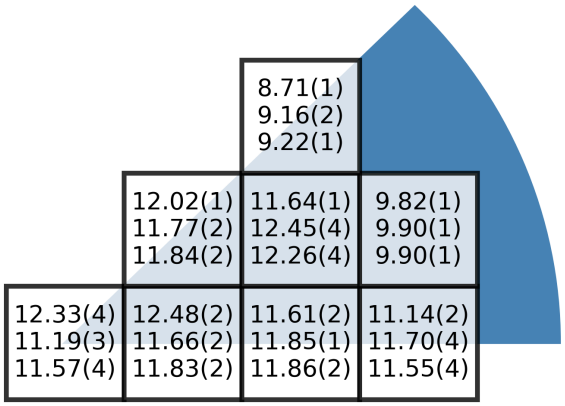

Figure 4: The ratio $S/\langle\phi\rangle_{core}$, i.e. between the assembly-wise neutron emission rate due to fission and the core-averaged flux, for each fuel assembly in the core. For each assembly, the ratio is shown for three points in time during the irradiation cycle: 0 days (top value), 365 days (middle value) and 730 days (bottom value). Statistical uncertainties are shown in parentheses. The blue wedge is not related to the model, but only shows the limits of the 1/8 core symmetry.

5.4. Leakage-energy dependence of detectable neutron flux

In order to investigate how neutrons having different energies when leaving the barrel contribute to the neutron flux at the detector location, the detector flagging capability of Serpent was used. At the core barrel, the energy of each leakage neutron was determined. For each 0.5-MeV interval of leakage-neutron energy, the contribution to the total neutron flux at the detector location was determined for the BOC core. The results (normalised to the total flux at the detector location) are shown in Fig. 5, and demonstrate that only neutrons with a sufficiently

high energy when leaving the core will provide a significant contribution to the total flux at the detector. The further from the core the detector is placed, the higher the leakage energy required to contribute to neutron flux at the detector location. The data shown in Fig. 5 are related to the weighting functions described above, but also incorporate information about the neutron emission spectrum (high-energy neutrons are less likely to be emitted in the fuel but have a higher probability of reaching the detector). These results show that the ratio $\langle\phi\rangle_{det}/\langle\phi\rangle_{core}$ depends not only on the spatial distribution of S, but also on the energy distribution of S (a neutron emitted close to the periphery has a relatively high probability of reaching the detector, but even more so if this is a high-energy neutron). The consequence is that it is also important to understand how the high-energy tail of the fission-neutron spectrum in the fuel changes with burnup — for example the fission-neutron emission spectrum for plutonium that builds up during operation has a slightly larger high-energy tail than the uranium in the fresh fuel.

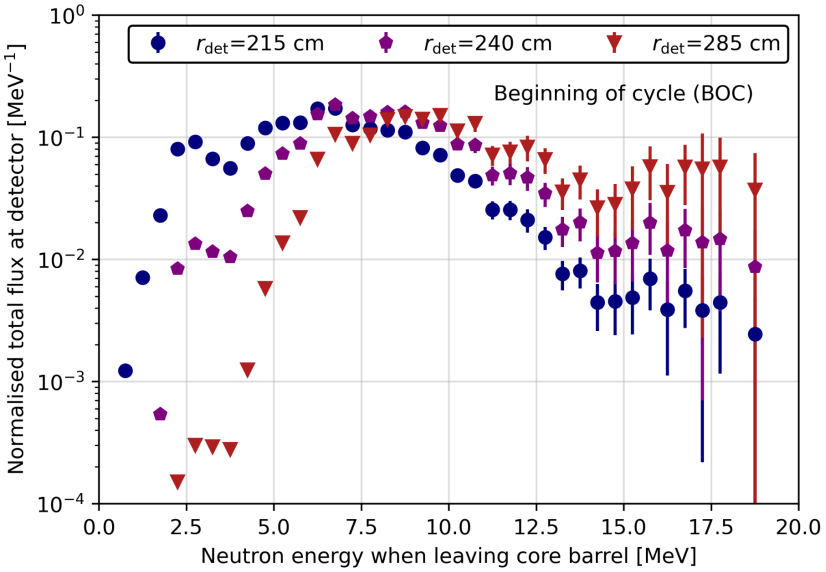

Figure 5: The total neutron flux at various detector locations, as function of the neutron energy when exiting the core barrel. The data, which are for the BOC core (0 days), have been normalised to the total flux at each detector location. As the distance from the core increases, the importance of high-energy neutrons increases. This can be observed as a clear change in the low-energy part of the distribution.

6. Discussion and Conclusion

In this work, the very first irradiation cycle of a NuScale iPWR SMR has been modelled to study how the neutron flux outside the core CNV changes during a two-year irradiation cycle. Earlier studies have proposed monitoring of such leakage neutrons over time to provide safeguards information about the composition of the core over time. The results presented in this paper indicate that the long-term variations in the neutron flux outside a nuclear reactor is not only related to the reactor power and average fissile composition of the core, but also to the spatial and energy distribution of the fission neutron source in the core. This is in turn related to the flux and power distribution in the core, all which may vary over time. This means that the relationship between the core-averaged flux and the detected flux is not independent of time.

Simulations in this work show that fuel depletion does indeed affect the neutron flux outside the core. This change could be detected to indicate possible undeclared activities in the facility. However, more careful analysis is needed of how changes in flux, fuel composition and other parameters throughout the core impact the measurable neutron signatures.

Future work could focus on establishing a model including assemblies which have already been in the core for one or more cycles, which might remove potential effects in the results which are due to the initial build-up of radionuclides in the core. Nonetheless, some variations in both the spatial and energy distribution of the fission neutron source over an irradiation cycle is expected also in a more realistic scenario. The results presented here could also serve as a first basis for selecting a detector capable of detecting changes in neutron flux with sufficient accuracy.

Finally, we note that understanding the behaviour of fast neutrons outside the core is key to understanding how the detected neutron signal relates to the composition of the core. Monitoring of the core at even larger distances, such as proposed in [3], depends to a large extent on the transport and slowing down of fast neutrons when passing through additional structural material outside the reactor. After selecting an appropriate detector technology and positioning, energy-dependent weighting functions should be determined. The computational performance of future work could likely be optimised by implementing energy-dependent variance reduction.

7. Acknowledgements

This work was funded by the Swedish Radiation Safety Authority (SSM) under agreement SSM2022-4034.

8. References

[1] S. Prasad et al., “Nonproliferation improvements and challenges presented by small modular reactors,” Prog. Nucl. Energ., vol. 80, pp. 102-109, Apr. 2015.
[2] A. Bernstein et al., “Colloquium: Neutrino detectors as tools for nuclear security,” Rev. Mod. Phys., vol. 92, art. no. 011003, Jan.-Mar. 2020.
[3] B. M. van der Ende et al., “Stand-off nuclear reactor monitoring with neutron detectors for safeguards and non-proliferation applications,” Nat. Commun., vol. 10, art. no. 1959, 2019.
[4] IAEA Department of Safeguards, “Long-Term R&D Plan, 2012-2023, “ IAEA, Vienna, Austria, Jan. 2013.
[5] United States Nuclear Regulatory Commission. “Application Documents for the NuScale US600 Design.” Last modified February 17, 2023. https://www.nrc.gov/reactors/new-reactors/smr/licensing-activities/nuscale/documents.html.
[6] M. Pecchia et al., “A methodology for evaluating weighting functions using MCNP and its application to PWR ex-core analyses,” Ann. Nucl. Energy, vol. 105, pp. 121-132, July 2017.
[7] P. Suk et al., “Simulation of a NuScale core design with the CASL VERA code,” Nucl. Eng. Design, vol. 371, 110956, Jan. 2021.
[8] J. Leppänen et al., “The Serpent Monte Carlo code: Status, development and applications in 2013,” Ann. Nucl. Energy, vol. 82, pp. 142-150, Aug. 2015.
[9] J. Leppänen, “Response Matrix Method–Based Importance Solver and Variance Reduction Scheme in the Serpent 2 Monte Carlo Code,” Nucl. Technol., vol. 205, no. 11, pp. 1416-1432, Nov. 2019.